Mechanical Systems and Signal Processing 201 (2023) 110675

Contents lists available at ScienceDirect

Mechanical Systems and Signal Processing

journal homepage: www.elsevier.com/locate/ymssp

A novel resonant frequency tracking technique for linear compressors

Zhennan Zhu [a,d], Kun Liang [b,a,*], Zhaohua Li [b,*], Hongyue Chen [c]

[a] Department of Engineering and Design, University of Sussex, Brighton BN1 9QT, UK
[b] College of Mechanical Engineering, Yangzhou University, Yangzhou 225012, China
[c] School of Mechanical Engineering, Liaoning Technical University, Fuxin 123000, China
[d] Department of Chemical Engineering, Imperial College London, London SW7 2AZ, UK

ARTICLE INFO

Keywords:
Linear compressor
Resonant frequency tracking
Observer
Phase detection
PI controller

ABSTRACT

Linear compressors are more efficient than conventional reciprocating com- pressors due to the absence of a crank mechanism. One of the main challenges for linear compressors is to keep operating at resonant frequency to maximise the efficiency. In this study, a novel resonant frequency tracking method that keeps the current and piston velocity in phase is proposed using a numerical linear compressor model with two Luenberger observers for the current and piston velocity, a zero-crossing detector for the phase difference and a PI (proportional-integral) controller updating the operating frequency. Experiments are conducted using R134a for model verification. The observers can give good prediction of the current and piston velocity while the phase detector and the PI controller are capable of adjusting the operating frequency to resonance with an uncertainty less than 1% compared to the experiments. Resonant operation can achieve the smallest current amplitude thus a lower power consumption.

1. Introduction

Linear compressor, which has no crank mechanism, is an increasing research interest and has a wide range of applications such as Stirling cryocoolers, Joule Thomson coolers and vapour compression refrigeration (VCR) systems [1]. Compared with a conventional rotary compressor, a linear compressor utilizes a linear reciprocating motor and allows free-piston operation, leading to the advantages of compact scale, low noise, and oil-free operation thus much lower friction [2–4]. A linear compressor is usually able to achieve 10% ~20% higher efficiency and lower energy consumption especially at part-load conditions [5,6] as well as mitigating CO_2 emission [7]. Another advantage of the linear compressor is the capacity modulation resulting from the variable displacement.

Unlike conventional compressors under the constraint of the crank mechanism, linear compressors can alter the compressor stroke to meet different cooling demands [8]. However, this may result in an off-resonance operating frequency. As it has been proven that the electromagnetic force is minimal when the oscillation frequency equals the resonant frequency [9], functioning at an off-resonant frequency would result in higher power consumption and worse efficiency. The resonant frequency can be calculated using the following equation [10]:

$$f_{\mathrm{res}} = (1/2\pi)\sqrt{k_{\mathrm{total}}/m} \tag{1}$$

* Corresponding authors at: College of Mechanical Engineering, Yangzhou University, Yangzhou 225012, China (K. Liang).
E-mail addresses: kun.liang@sussex.ac.uk (K. Liang), zhaohua.li@yzu.edu.cn (Z. Li).

https://doi.org/10.1016/j.ymssp.2023.110675
Received 21 April 2023; Received in revised form 19 July 2023; Accepted 5 August 2023
Available online 10 August 2023

Nomenclature

Abbreviation

A_p	Area of piston (m^2)
C	Capacitance (F)
CD	Damping coefficient (N*s/m)
CL	Clearance (mm)
CoP	Coefficient of performance
e	Specific internal energy (J/kg)
D_p	Diameter of piston (mm)
E	Internal energy (J)
f	Frequency (Hz)
f_{res}	Resonant frequency (Hz)
F	Force (N)
h	Enthalpy (kJ/kg)
i	Current (A)
k_{gas}	Gas spring stiffness (N/m)
k_s	Mechanical stiffness (N/m)
L	Inductance (H)
L_p	Length of piston (mm)
M	Mass (kg)
P	Pressure (bar)
$\dot{Q}$	Heat transfer (W)
R	Resistance (Ω)
T	Temperature (K)
U	Voltage (V)
$\dot{W}$	Power (W)
X	Displacement (mm)
$\dot{X}$	Velocity (m/s)
$\ddot{X}$	Acceleration (m/s^2)

Greeks

α	Motor constant (N/A)
μ	Viscosity (Pa·s)

$$k_{total} = k_s + k_{gas} \tag{2}$$

where k_s and k_{gas} denote the mechanical and gas spring stiffness, k_{total} denotes the total spring stiffness. It is seen that the resonant frequency of a linear compressor is determined by the spring stiffness including the mechanical spring and gas spring because the moving mass is a constant [11]. A change in compressor stroke will bring a corresponding change in the gas spring stiffness. There are two approaches to help the linear compressor keep resonant. The first is to raise the stiffness for the mechanical spring to dominate the resonance thus the varying in gas spring stiffness will be negligible. The second is to continually adjust the operating frequency to resonance when the working condition varies. LG linear compressor follows the first logic by using several helical compression coil springs [12]. However, this will make the compressor exceedingly heavy and inconvenient to transport. As a result, resonant frequency tracking techniques for linear compressors are required to ensure that they operate at resonance regardless of operational variables such as varying strokes, temperatures, and pressures.

The gas spring stiffness, which varies with the cooling load, is a non-linear function against the piston stroke [13]. Bradshaw et al. [14] and Liang [15] also pointed out that the resonant frequency was a non-linear function of the stroke-to-diameter ratio. It is a challenge to achieve the resonance by directly computing the gas spring stiffness in real time.

To date, there are several works relating to the resonant frequency tracking of linear compressors. Lin et al. [13] developed a resonance tracking method by finding the maximum power for a given current amplitude. It was found that the resonance brought the linear compressor its maximum stroke and output power. However, as the maximum output power is difficult to be previously known, it will increase the difficulty in designing of the controller. Yu et al. [16] numerically studied the resonant frequency tracking strategy by finding the minimum current. However, as the maximum power and minimum current are not known in advance, many loops are needed thus a very long settling time. Besides, the compressor stroke and other operating parameters such as pressures and temperatures of heat exchangers may not be constant. Xu et al. [17] established a model reference adaptive system to adjust the spring stiffness and the damping ratio to make the piston velocity from the adjustable model agree with that from the reference model. This method is novel but requires a highly accurate reference model. The thermodynamic process of the linear compressor was simplified as

well.

To improve that, researchers proposed methods with a certain reference to be the criterion of resonance such as the phase angle. References [18,24] use the 90° phase angle between the piston displacement and the voltage (or current) as the criterion of resonance. However, Suzuki et al. [18] utilizes a Fourier transformation to define the piston position thus presents complicated calculation while the linear compressor model of Chun et al. [19] and Zhang et al. [20] lacks the in-cylinder thermodynamics process thus increases inaccuracy. Moreover, the wave fitting phase detection method in [20] requires complex computing. Chun et al. [21] also has key shortcomings such as that the initial stage of these signals is not stable if the operating frequency changes and the linear compressor model is simplified. Latham et al. [22,23] established nonlinear observers to obtain parameters such as the piston velocity, acceleration and top and bottom dead centres. However, the linear compressor behaviour was just described by a piston dynamic model and an electrical model without capacitor. Xu et al. [24] established an adaptive full-order displacement observer to achieve the resonant frequency tracking for a linear compressor, showing good agreement but complex calculation. There was no thermodynamic sub-model as well.

In summary, linear compressors can generally present higher efficiency over conventional ones. By using resonant frequency tracking technology, the motor efficiency of a linear compressor can be kept at a high level thus the compressor efficiency can be further improved. Although there are already many studies on resonant frequency tracking, they all have shortcomings such as simplified linear compressor model [17,19–23] thus low accuracy as well as complex calculations [13,16,18,24]. Additionally, most of these studies chose the phase of piston displacement for calculation [18,24]. This will further reduce the accuracy of tracking because the piston displacement may have DC bias (piston offset) due to the pressure difference between the two sides of the piston. Following the theory that the phase angle between piston displacement and current reaches 90° when resonance, it is also known that the piston velocity and current are in phase when resonance. As a result, it is necessary to provide a resonant frequency tracking method that can be broadly applied in linear compressors and should have high accuracy and simple calculation.

In this study, a resonant frequency tracking strategy is proposed based on an accurate model of linear compressor with observing the current and piston velocity. In Section 2, the linear compressor model illustrating the in-cylinder thermodynamic process, the piston motion, and the electrical behaviour is built. Two Luenberger observers describing the piston motion, and the electrical behaviour are established to replace the iterative computations by two state-space equations. In Section 3, a novel resonant frequency tracking method is proposed and numerically studied with a zero-crossing detection for the phase angle between piston velocity and current and a PI controller that changes the frequency. In Section 4, the experimental apparatus and method that verify the accuracy of the linear compressor model and observers are introduced. This numerical study can achieve the resonant frequency tracking without complex calculations as well as provide the reference for the practical use.

2. Linear compressor model

2.1. Compressor sub-models

The linear compressor model contains three major parts named the thermodynamic sub-model, the piston dynamics sub-model and the electrical motor sub-model, respectively. NIST REFPROP database is used to obtain the properties of the working fluid [25].

2.1.1. Thermodynamic sub-model

The change of the in-cylinder temperature and pressure is described using a thermodynamic sub-model based on mass and energy conservation theory, which can be written as follows:

$$\frac{dE}{dt} = \dot{Q} + \dot{W} + \sum_{in} \dot{m}_{in} h_{in} - \sum_{out} \dot{m}_{out} h_{out} \tag{3}$$

$$\frac{dE}{dt} = \frac{d(e_c m_c)}{dt} = m_c \frac{de_c}{dt} + e_c \frac{dm_c}{dt} \tag{4}$$

where $\dot{Q}$ and $\dot{W}$ denote the heat exchange and the shaft work per time step. $\dot{m}_{in}$ and $\dot{m}_{out}$ are the mass flow rate into and out of the compression chamber of the linear compressor (space between the piston and the valves in Figure 1) while h_{in} and h_{out} donate the enthalpy of the refrigerant flowing into and out of the compression chamber. It is worth noting that $\dot{m}_{out}$ is the mass flow rate that join

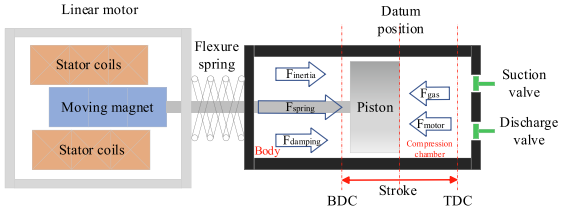

Fig. 1. Schematic of the linear compressor (compression chamber, body chamber and the linear motor. BDC: Bottom dead centre; TDC: Top dead centre).

the cycle of the refrigeration system. m_c and e_c respectively represent the refrigerant mass and the specific internal energy in the compression chamber, which can be expressed as below:

$$de = c_v dT \tag{5}$$

$$e = h - PV \tag{6}$$

where c_v denotes the specific heat capacity at constant volume, T is the temperature, P is the pressure, h represents the specific enthalpy of the refrigerant in the compression chamber, v is the specific volume expressed as

$$v = 1/\rho \tag{7}$$

The shaft power $\dot{W}$ can be expressed as

$$\dot{W} = -P\left(\frac{dV}{dT}\right) \tag{8}$$

An expression of the temperature change in compression chamber can be obtained by combining Eqs. (3)–(8):

$$\frac{dT_c}{dt} = \frac{1}{m_c c_v}\left[\dot{Q} + \sum_{in}\dot{m}_{in}h_{in} - \sum_{out}\dot{m}_{out}h_{out} - h_c\frac{dm_c}{dt} - T_c\left(\frac{\partial P}{\partial T}\right)_V\left(\frac{dV_c}{dt} - \frac{1}{\rho}\frac{dm_c}{dt}\right)\right] \tag{9}$$

The in-cylinder temperature can be calculated by adding the temperature change to the temperature in the last step. The in-cylinder pressure can then be obtained using REFPROP database [25] in MATLAB/Simulink environment.

It is needed to take the seal leakage $\dot{m}_{leak}$ into account when calculating $\dot{m}_{in}$ and $\dot{m}_{out}$. An equation proposed by Liang [26] can be applied, shown as

$$\dot{m}_{leak} = \frac{\pi D_p CL^3\left(P_c^2 - P_b^2\right)}{24\mu L_p R_g T_c} \tag{10}$$

where D_p and L_p represent the piston diameter and length, CL denotes the clearance.

A heat transfer model is proposed by using the instantaneous heat transfer coefficient equation (Eq.(11)) from [27] to calculate the heat exchange $\dot{Q}$.

$$h_t = \left(0.28Re^{0.65} + 0.25z\frac{T_w}{T_c - T_w}\right)\left(\frac{k}{D_p}\right) \tag{11}$$

where h_t is the instantaneous heat transfer coefficient, Re is the Reynold number, z is the compressibility factor, T_w is the cylinder wall temperature, and k is the thermal conductivity.

The Re and z can be calculated as

$$Re = \rho\left|\dot{X}_p\right|D_p \Big/ \mu \tag{12}$$

$$z = \frac{\gamma - 1}{V_c}\frac{dV_c}{dt}\sqrt{\frac{D_p^3}{\alpha\left|\dot{X}_p\right|}} \tag{13}$$

where μ is the viscosity and α is the gas diffusivity.

The heat exchange $\dot{Q}$ can be expressed as

$$\dot{Q} = h_t A(T_c - T_w)\Big/ dt \tag{14}$$

where A is the heat exchange area, which can be expressed as Eq.(15). The number 0.00757 denotes the datum position of the piston.

$$A = \pi D_p^2\left(X_p + 0.00757\right) \tag{15}$$

2.1.2. Piston dynamics sub-model

A piston dynamics sub-model can describe the forces affecting the piston behaviour, shown in Figure 1. The piston is acted upon by the motor force F_{motor}, the damping force $F_{damping}$, the spring force F_{spring}, and the gas force F_{gas}. The resultant force $F_{inertia}$ is the vector sum of the forces above. F_{motor} is the driving power source provided by the motor and always in the same direction of the piston motion while $F_{damping}$ is opposite. F_{spring} is to make the piston back to the datum position, which is provided by the flexure spring. F_{gas} is due to the pressure difference on two sides of the piston. The piston dynamics sub-model can be written as

$$F_{\text{motor}} + F_{\text{gas}} = M_{\text{p}}\ddot{X}_{\text{p}} + CD_{\text{p}}\dot{X}_{\text{p}} + k_{\text{s}}X_{\text{p}} \tag{16}$$

$$F_{\text{motor}} = \alpha i \tag{17}$$

where M_{p} is the mass of piston, CD_{p} is the damping ratio, k_{s} is the spring stiffness, α and i represent the motor constant through correlation [26] and the current, respectively. X_{p}, $\dot{X}_{\text{p}}$ and $\ddot{X}_{\text{p}}$ denote the displacement, velocity and acceleration of the piston, respectively.

2.1.3. Electrical motor sub-model

The linear motor's electrical behaviour can be represented using an RLC circuit with a capacitor to eliminate the phase shift induced by the inductor [7,9,21,24,26], as seen in Figure 2 and written as

$$U - \text{BEMF} = \text{R}i + \text{L}\left(\text{d}i \Big/ \text{d}t\right) + \left(1 \Big/ \text{C}\right) \int i\text{d}t \tag{18}$$

$$\text{BEMF} = \alpha\dot{X}_{\text{p}} \tag{19}$$

where U is the input voltage, R, L and C represent the resistance, inductance and capacitance, respectively, and BEMF represents the back electromotive force. It is worth to note that the R, L and C are fixed values thus the LC resonant frequency is also fixed, and the resonant frequency needed to be satisfied is the mechanical resonant frequency mentioned in Eq.(1).

2.2. Observers for current and piston velocity

Using observers can help the state estimation, increasing flexibility and sensor Redundancy for the model-based control [27,28]. Moreover, many iterative computations are necessary to calculate the parameters in the numerical model (for example, the piston displacement: $X_{\text{p}}^{\text{n+1}} = X_{\text{p}}^{\text{n}} + \dot{X}_{\text{p}}^{\text{n}}\text{d}t + \frac{1}{2}\ddot{X}_{\text{p}}^{\text{n}}\text{d}t^2$), resulting in increased complexity. Luenberger observer is a linear observer that can significantly simplify the modelling with keeping the accuracy. In this study, the piston dynamics sub-model and the electrical motor sub-model are stated using state-spaces and two Luenberger observers. Following this method, Eq.(16) and (18) can be rewritten as:

$$F_{\text{in}} = M_{\text{p}}\ddot{X}_{\text{p}} + \text{CD}_{\text{p}}\dot{X}_{\text{p}} + k_{\text{s}}X_{\text{p}} \tag{20}$$

$$U_{\text{in}} = \text{R}i + \text{L}(\text{d}i/\text{d}t) + (1/\text{C}) \int i\text{d}t \tag{21}$$

where $F_{\text{in}} = F_{\text{motor}} + F_{\text{gas}}$, $U_{in} = U - \text{BEMF}$. For the piston dynamics sub-model, set the displacement and the velocity as the states (Z_1 and Z_2), the displacement as the output (y), and resultant force of motor force and gas force as the input (u), thus:

$$Z_1 = X_{\text{p}} \tag{22}$$

$$Z_2 = \dot{X}_{\text{p}} \tag{23}$$

$$y = X_{\text{p}} \tag{24}$$

$$u = F_{\text{in}} \tag{25}$$

Then Eq. (20) can be rewritten as

$$\begin{bmatrix} \dot{Z}_1 \\ \dot{Z}_2 \end{bmatrix} = \begin{bmatrix} 0 & 1 \\ -k_{\text{s}}/M_{\text{p}} & -\text{CD}_{\text{p}}/M_{\text{p}} \end{bmatrix} \begin{bmatrix} Z_1 \\ Z_2 \end{bmatrix} + \begin{bmatrix} 0 \\ 1/M_{\text{p}} \end{bmatrix} u \tag{26}$$

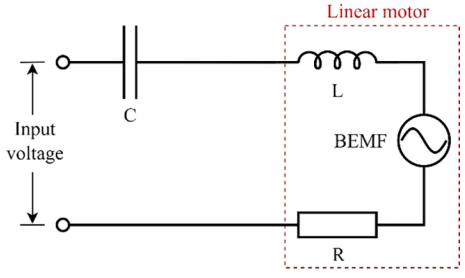

Fig. 2. Equivalent circuit of the linear motor.

$$y = [1 \quad 0]\begin{bmatrix} Z_1 \\ Z_2 \end{bmatrix} + [0]u \tag{27}$$

Set $L_{\text{mech}} = \begin{bmatrix} L_1 \\ L_2 \end{bmatrix}$ and the state-space equations can be expressed in the format of an observer, the estimated parameters are marked with a hat:

$$\dot{\widehat{Z}} = (A - L_{\text{mech}}C)\widehat{Z} + (B - L_{\text{mech}}D)u + L_{\text{mech}}y \tag{28}$$

where $A = \begin{bmatrix} 0 & 1 \\ -k_s/M_p & -CD_p/M_p \end{bmatrix}$, $B = \begin{bmatrix} 0 \\ 1/M_p \end{bmatrix}$, $C = [1 \quad 0]$ and $D = [0]$.

The observability can be confirmed through following steps:

From Eq.(26) and (27), the observability matrix should be formed by stacking the matrices $[1 \quad 0]$ and $[1 \quad 0]\begin{bmatrix} 0 & 1 \\ -k_s/M_p & -CD_p/M_p \end{bmatrix}$ ($O = \begin{bmatrix} C \\ CA \end{bmatrix}$). Therefore, the observability matrix is as

$$O_{\text{mech}} = \begin{bmatrix} 1 & 0 \\ 0 & 1 \end{bmatrix} \tag{29}$$

It can be seen that the rank of this matrix is 2, which equals to the number of states. Therefore, the system is fully observable, and all states can be uniquely estimated from the outputs.

To ensure the stability of the system, the eigenvalues of $(A - L_{\text{mech}}C)$ should have negative real parts. The eigenvalues of $(A - L_{\text{mech}}C)$ correspond to the system's characteristic roots or poles. Stability requires that all these eigenvalues have negative real parts. When the real parts of the eigenvalues are negative, it indicates that the system's response will decay over time, leading to a stable and well-behaved system. Positive real parts in the eigenvalues imply that the system's response will grow or oscillate, indicating instability. Therefore, for Eq.(28), set $\lambda_1 = \lambda_2 = -1$, L_{mech} can be calculated as

$$|\lambda I - (A - L_{\text{mech}}C)| = 0 \tag{30}$$

where I is the unit matrix. Then L_{mech} can be expressed as (the subscript 'mech' indicates the mechanical dynamic sub-model)

$$L_{\text{mech}} = \begin{bmatrix} L_1 \\ L_2 \end{bmatrix} = \begin{bmatrix} 2 - CD_p/M_p \\ 1 - (k_s + 2CD_p + CD_p^2)/M_p \end{bmatrix} \tag{31}$$

Substituting Eq. (31) to (28), the observer for the piston dynamics sub-model is expressed as

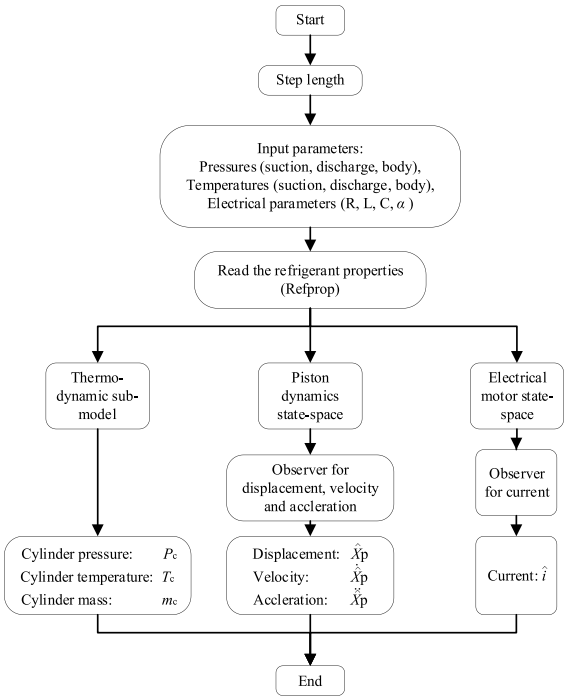

Fig. 3. Schematic of the linear compressor model and associated observers.

$$\begin{bmatrix}\dot{\hat{Z}}_1\\ \dot{\hat{Z}}_2\end{bmatrix}=\begin{bmatrix}-L_1 & 1\\ -\frac{k_s}{M_p}-L_2 & -\frac{CD_p}{M_p}\end{bmatrix}\begin{bmatrix}\hat{Z}_1\\ \hat{Z}_2\end{bmatrix}+\begin{bmatrix}0\\ \frac{1}{M_p}\end{bmatrix}u+\begin{bmatrix}L_1\\ L_2\end{bmatrix}y \tag{32}$$

Likewise, the observability matrix for the electrical motor sub-model (Eq.(33)) and the observer for the electrical motor sub-model can be obtained. It can be seen that the rank of the observability matrix is 2 thus fully observable. Set the voltage of the capacitor and the current as states, the current as the output, and U_{in} as the input, and the observer can be expressed as Eq.(34) and (35) (the subscript'elec' indicates the electrical motor sub-model):

$$O_{elec}=\begin{bmatrix}1 & 0\\ 0 & 1/C\end{bmatrix} \tag{33}$$

$$L_{elec}=\begin{bmatrix}L_3\\ L_4\end{bmatrix}=\begin{bmatrix}1/C-L\\ 2-R/L\end{bmatrix} \tag{34}$$

$$\begin{bmatrix}\dot{\hat{Z}}_3\\ \dot{\hat{Z}}_4\end{bmatrix}=\begin{bmatrix}0 & \frac{1}{C}-L_1\\ -\frac{1}{L} & \frac{R}{L}-L_2\end{bmatrix}\begin{bmatrix}\hat{Z}_3\\ \hat{Z}_4\end{bmatrix}+\begin{bmatrix}0\\ \frac{1}{L}\end{bmatrix}u+\begin{bmatrix}L_3\\ L_4\end{bmatrix}y \tag{35}$$

The diagram of the linear compressor model illustrating the implementation is shown in Figure 3. The linear compressor model, observers and the controller are integrated in a MATLAB/Simulink environment.

3. Resonant frequency tracking strategy

The resonant frequency tracking strategy in this study is to control the phase difference. For the sinusoidal signals, a very common method to measure the phase difference between two signals is the zero-crossing method, which calculates the time difference between the two signals becoming positive one after the other. The diagram of zero-crossing phase detector is shown as Figure 4.

An integral of 1 was applied to compute the time difference. When signal 1 (the blue solid line) becomes positive, the integral will be triggered. The integral calculation will last until signal 2 (the red dash line) becomes positive. Thus, the time difference can be

$$t_{diff}=\int_{t_{trigger}}^{t_{stop}}1\mathrm{d}t=t_{stop}-t_{trigger} \tag{34}$$

As the zero-crossing test requires a certain datum position to ensure the accuracy, a considerable offset is not acceptable. However, due to the integral calculation, the displacement has an offset which cannot be predicted. To avoid this uncertainty, the phase difference between the piston velocity and the current are chosen as the criterion. After the piston velocity signal and the current signal are computed through the linear compressor model, they are passed to the zero-crossing phase detector to calculate the phase angle, seen as

$$\Phi_{diff}=\Phi_i-\Phi_{\dot{x}} \tag{35}$$

The phase difference in degree can be calculated as

$$\Phi_{diff}=t_{diff}\tilde{A}\cdot(1/f)\times 360 \tag{36}$$

A reference phase angle $\Phi_{ref}=0$ is set to obtain the error in phase Δe_Φ, expressed as

$$\Delta e_\Phi=\Phi_{ref}-\Phi_{diff} \tag{37}$$

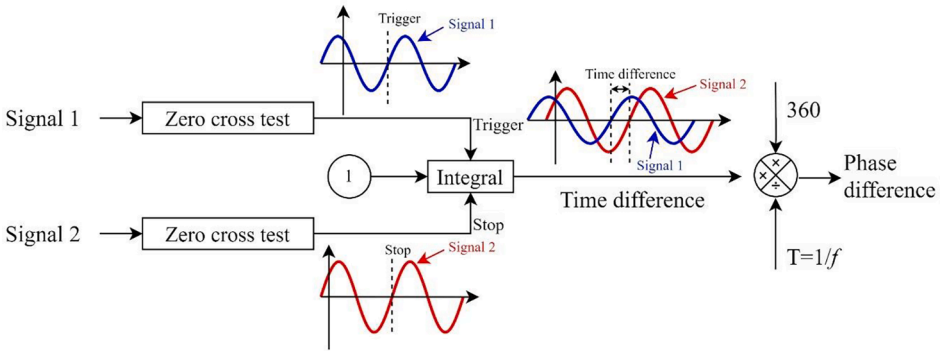

Fig. 4. The diagram of zero-crossing phase detector.

A PI controller is employed to adjust the frequency as below. Note that the phase difference can only be obtained when the signals are stable, the PI controller is set to function every 0.3 s as it is observed that the signals become stable after this period. Therefore, the frequency is adjusted discretely. The subscript k denotes the kth time step:

$$\Delta f = \mathrm{PI}(\Delta e_{\Phi}) \tag{38}$$

$$f_{k+1} = f_k + \Delta f \tag{39}$$

Figure 5 shows the diagram of the resonant frequency tracking technique, which mainly consists of three steps as below: 1) current and piston velocity calculation by the linear compressor model; 2) phase difference detection by the zero-crossing phase detector; 3) operating frequency adjusting by the PI controller. The detailed procedure is as follows: if $\Delta e_{\Phi} > 0$, indicating a negative Φ_{diff}, meaning the current lags the velocity, the operating frequency should be increased with a positive Δf. If $\Delta e_{\Phi} < 0$, indicating a positive Φ_{diff}, meaning the current leading the velocity, the operating frequency should be decreased with a negative Δf. If $\Delta e_{\Phi} = 0$, meaning the current and the velocity are in phase, the operating frequency should be unchanged with $\Delta f = 0$.

4. Experiments

To verify the linear compressor model, experiments were done utilising a linear compressor vapour compression test apparatus with R134a as the refrigerant. A linear compressor driven by a moving magnet linear motor was built, which includes a piston mechanical assembly, two flexure springs and two reed valves for suction and discharge. The piston mechanical assembly is regarded as a spring-damp system locating in the cylinder as shown in Eq.(16) and Figure 1. The linear motor consists of a resistance and an inductance with an extra capacitance added, which is illustrated in Eq.(18) and Figure 2. Figure 6 displays the prototype oil-free linear compressor and Table 1 lists the key parameters of the linear compressor.

The linear compressor VCR test rig is shown in Figure 7. The test rig consists of a VCR system (the black solid lines), a bleed flow pipeline (the orange solid lines) and a controlling and data acquisition system (the red dash lines).

The VCR system consists of two linear compressors oppositely arranged, an off-the-shelf copper water-cooled coaxial condenser, an expansion valve, and an evaporator with an electric heater inside. The key temperatures (suction, discharge, body, before and after the heat exchangers) were measured by seven K-type thermocouples with the accuracy of ± 1.5 ℃ while the key pressures (suction, discharge, body and after expansion) were measured by four Druck PMP1400 pressure transducers with a range of 0–25 bar. The main mass flow rate was measured using a Hastings HFM-201 thermal-type mass flow meter with an accuracy of ± 1%. The voltage and current were measured by a Fylde 261 HVA HV voltage attenuator and two LA LEM 25-NP current transducers for each linear compressor. Two data acquisition devices (DAQ) were adopted to obtain the signals of temperatures, pressures, mass flow rate and displacement, etc. The details of the test rig can be found in [26]. According to our previous uncertainty analysis, all inaccuracies in power input, cooling capacity, CoP, and volumetric efficiency of within 2% [29].

5. Results and discussion

5.1. Model validation

As mentioned in Section II. A, the thermodynamic sub-model gives the in-cylinder pressure. Figure 8 shows the *P-V* loop from both model and measurement [30]. A difference is seen at the high-pressure area, which is caused by the seal leakage of the reed valve. In general, a good agreement is observed. The current and velocity from measurement and observer are chosen to make the comparison to validate the feasibility and accuracy of the model as these two signals are essential for the resonant frequency tracking. Figure 9(a) displays the comparison between the current obtained by measurement and observer at the stroke of 10 mm, pressure ratio of 2.0 and condenser temperature of 50 °C. It is observed that the curve from the observer agrees well with the measured one. The error in amplitude is 5.2% while the error in phase is 0.3%. Figure 9(b) displays the comparison between the piston velocity obtained by measurement and observer at the stroke of 10 mm, pressure of 2.0 and condenser temperature of 50 °C. Like the current illustrated above, the curve from the observer agrees well with the measured one. The error in amplitude is 3.9% while the error in phase is 1%. It is considered that the accuracy of the model including the observer is sufficient for resonant frequency tracking and control.

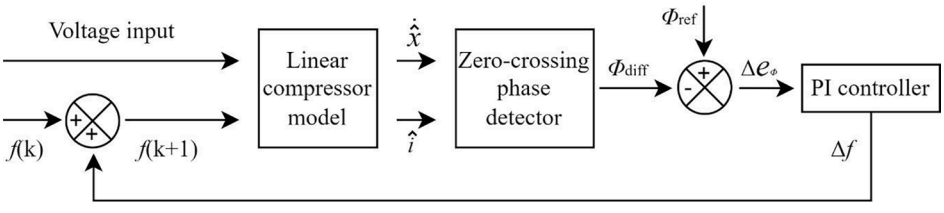

Fig. 5. The diagram of resonant frequency tracking technique.

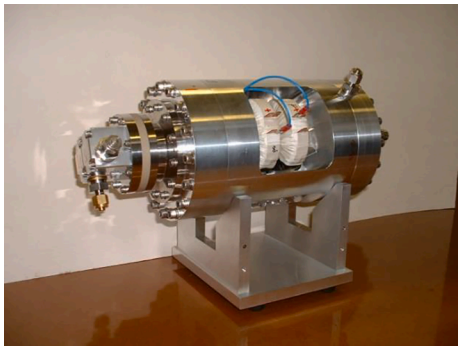

Fig. 6. Prototype oil-free linear compressor.

Table 1
Key parameters of the linear compressor.

Parameters	Values
Piston diameter (mm)	18.99
Piston length (mm)	31
Piston area (mm2)	283.23
Motor constant (N/A)	35
Moving mass (kg)	0.66
Mechanical Stiffness (N/m)	16284.85
Damping Coefficient (N·s/m)	0.0475
Resistance (Ω)	3.5
Inductance (H)	0.141
Capacitance (μF)	150

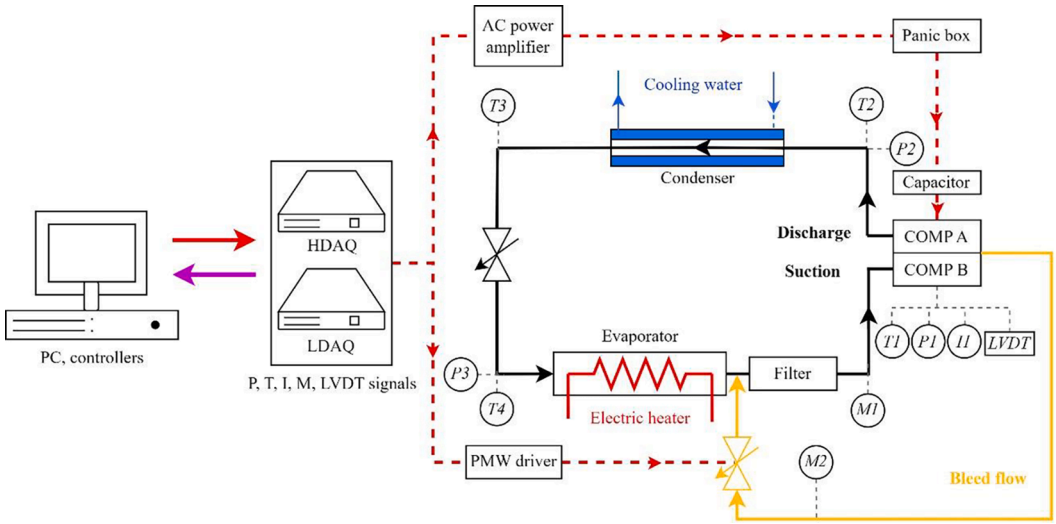

Fig. 7. Linear compressor vapour compression refrigeration test rig (P: pressure transducer, T: thermocouple, I: Current transducer, M: mass flow meter).

5.2. *Frequency tracking*

Figure 10 plots the frequency variation after the proposed resonant frequency tracking is applied at a stroke of 12 mm, condenser temperature of 50 °C and pressure ratio of 2.5 and 3.0, respectively. The red dash line represents the resonant frequencies that were experimentally identified. In the experiments, the resonant frequency was measured by changing the operating frequency to reach the highest motor efficiency. The adjust interval was firstly 1 Hz when the motor efficiency reached 90%, and then the increment was reduced to 0.5 Hz until lower motor efficiency occurred. The experimental error in resonant frequency was within 0.5 Hz. It is seen that with the resonant frequency tracking technique, the operating frequency can be adjusted to be very close to the resonant frequency.

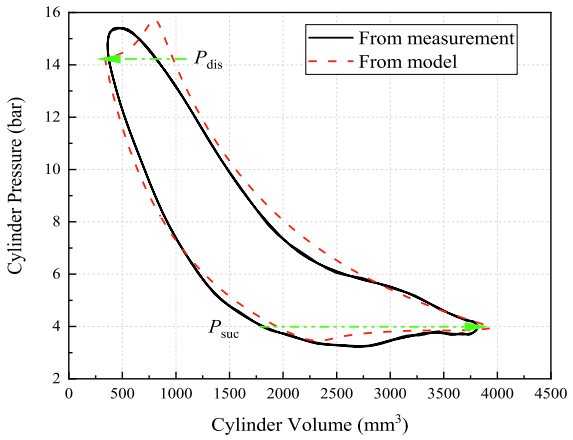

Fig. 8. P-V loop comparison between model and measurement using R134a at stroke of 12 mm, pressure ratio of 3.0 and condenser temperature of 50 °C [30].

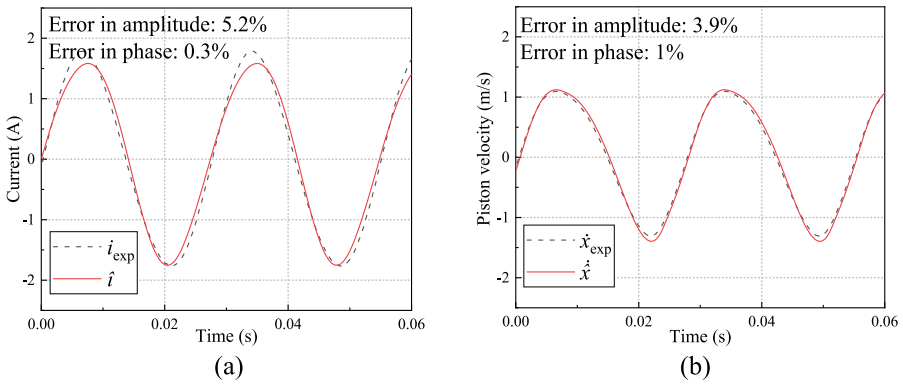

Fig. 9. Current and piston velocity from observers and measurement using R134a at stroke of 10 mm, pressure ratio of 2.0 and condenser temperature of 50 °C: (a) current (b) piston velocity.

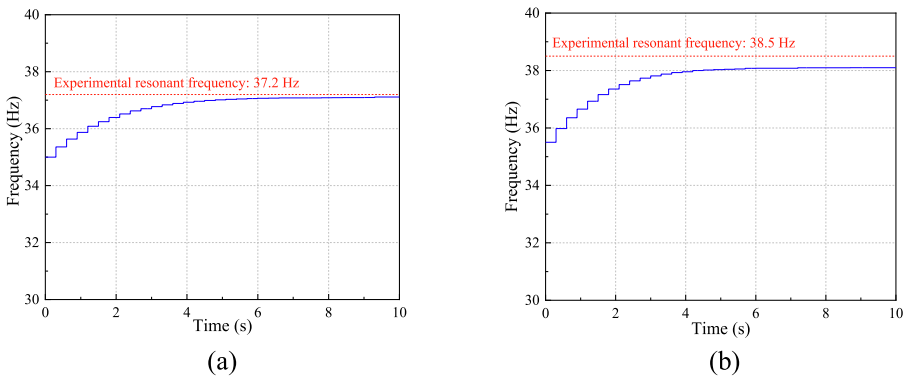

Fig. 10. Frequency variation under the resonant frequency tracking at stroke of 12 mm and condenser temperature of 50 °C: (a) pressure ratio 2.5 (b) pressure ratio 3.0.

The stable frequency at pressure ratio of 2.5 is 37.1 Hz while that at pressure ratio of 3.0 is 38.1 Hz. The differences between the tracked resonant frequencies and the experimental ones are 0.1 Hz (0.27%) and 0.4 Hz (1.04%), respectively.

Figure 11 plots the CoP (coefficient of performance) and electrical efficiency against drive frequency for a stroke of 11 mm and pressure ratio of 2.5 with an evaporator temperature of 19 °C and a condenser outlet temperature of 50 °C. It is observed that the CoP and electrical efficiency reach the highest values of 3.4 and 82% at resonant frequency (38 Hz). The CoP decreases to approximately

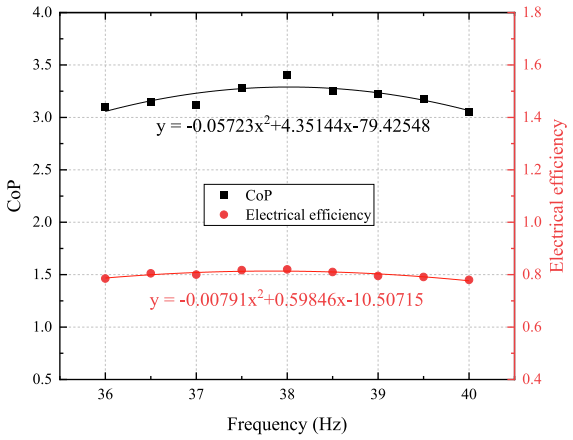

Fig. 11. CoP and electrical efficiency against drive frequency for a stroke of 11 mm and pressure ratio of 2.5 with an evaporator temperature of 19 °C and a condenser outlet temperature of 50 °C.

3.0 in both directions from the peak value when the operating frequency changes by 2 Hz. Similarly, the electrical efficiency decreases to 78% in both sides when the operating frequency is 2 Hz away from the resonance. This can verify the importance of operating at the resonant frequency. However, it can be seen that the curves are fairly flat, indicating that the operating frequency does not need to be precisely equal to the resonant frequency. Therefore, the final tracked resonant frequencies from the resonant frequency tracking technique (Figure 10) are acceptable.

5.3. Phase difference

Figure 12 display the frequency change and phase difference between current and piston velocity response of resonant frequency tracking at stroke of 11 mm, pressure ratio of 4.0 and condenser temperature of 50 °C starting with a lower and a higher operating frequency. It can be observed that the resonant frequency tracking method can work well both from a lower or higher initial frequency with decreasing Φ_{diff} and Δf to zero. It also can be seen that the settling time is different. It takes approximately 6 s when starting with 37.5 Hz, while 3 s when starting with 39.5 Hz. This is because that Δf is determined by Φ_{diff}. As observed, the phase differences are initially -17° and 25° when the operating frequencies are 37.5 Hz and 39.5 Hz respectively, and the PI controller gives larger Δf when starting with 39.5 Hz. This can also illustrate the robustness of the control strategy.

5.4. Effects of resonant frequency

Figure 13 illustrates the change in the curves of current and piston velocity at condenser temperature of 50 °C, pressure ratio of 4.0 and input voltage of 50 V. It is observed that when the operating frequency is significantly smaller than resonance (Figure 13(a)), the piston velocity leads the current by a significant phase angle. With the operating increasing towards the resonant frequency, the phase angle that the piston velocity leading the current becomes smaller (Figure 13(b)). After the operating frequency reaches resonant, the phase difference between the piston velocity and the current is negligible as they cross the zero point at almost the same time (Figure 13(c)). If the operating frequency continues increasing, the current will lag the piston velocity (Figure 13(d)(e)). It is seen that as the operating frequency varies towards resonance, the amplitude of the current decreases. The amplitude of the current decreases from 2.5 A at the operating frequency of 32 Hz to 0.8 A at the operating frequency of 38.25 Hz, then raises to 4.5 A at 44 Hz. Since the amplitude of the voltage is unchanged in the procedure of resonant frequency tracking, it can be deduced that the power consumption is lower when the system works at resonance, shown as Figure 14. The power consumption reaches the lowest of 40.1 W at resonance. When the operating frequency decreases to 32 Hz or raises to 44 Hz, the power consumption becomes 110.2 W and 207.2 W, respectively.

Figure 15 illustrates the resonant frequency as a function of piston stroke at different evaporator temperatures. When the condenser temperature is fixed, higher pressure indicates lower evaporator temperature. It is clear to see that the resonant frequency decreases with piston stroke increasing. This is because the increase in piston stroke brings a decreased stiffness of the gas spring, thus a lower effective spring stiffness. As the moving mass is considered as a constant, the resonant frequency decreases. Additionally, as the pressure ratio increases, the cylinder pressure becomes higher, leading to a higher gas spring stiffness, thus a higher resonant frequency. At the piston stroke of 11 mm, the resonant frequencies are 38.3 Hz and 38 Hz and 37.8 Hz for pressure ratio of 4.0, 3.5 and 3.0, decreases by 0.8% and 0.5%, respectively.

6. Conclusions

This work proposed a novel resonant frequency tracking strategy by keeping the current and piston velocity in phase. The

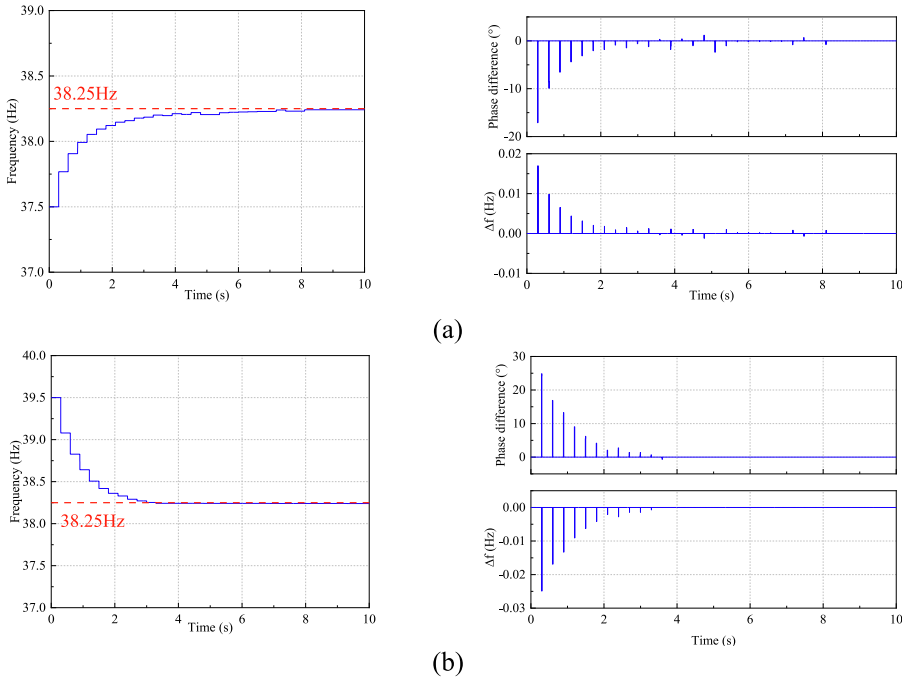

Fig. 12. Frequency change and phase difference between current and piston velocity response of resonant frequency tracking at stroke of 11 mm, pressure ratio of 4.0 and condenser temperature of 50 °C: (a) starting with a lower frequency (b) starting with a higher frequency.

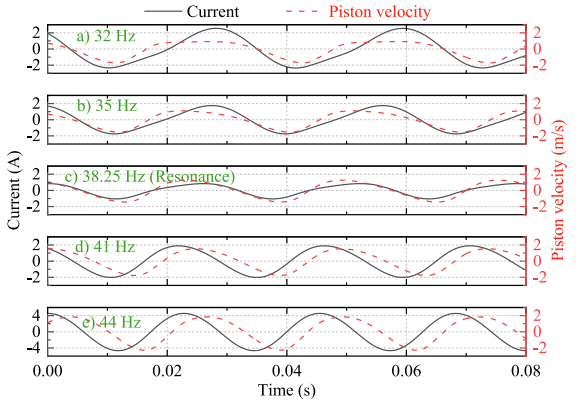

Fig. 13. Phase difference between current and piston velocity before and after reaching resonance at condenser temperature of 50 °C, pressure ratio of 4.0 and input voltage of 50 V.

characteristics of resonant frequency tracking for the linear compressor are numerically investigated. Here are the main findings:

1) The linear compressor model and the observers can give an accurate prediction of the current and piston velocity with errors in amplitude and phase smaller than 5% and 1%, respectively.
2) The resonant frequency tracking method can help adjust the operating frequency to resonance with an error smaller than 1%, which has a negligible effect on the CoP and power consumption of the linear compressor.
3) The amplitude of current will decrease when operating frequency varies towards resonance. At the condenser temperature of 50 °C, pressure ratio of 4.0 and input voltage of 50 V, the amplitude of the current decreases from 2.5 A at the operating frequency of 32 Hz to 0.8 A at the operating frequency of 38.25 Hz, then raises to 4.5 A at 44 Hz.
4) Higher pressure ratio can lead to higher resonant frequency as well as smaller piston stroke. The resonant frequency ranges within 36 Hz to 39 Hz when the pressure ratio is within 3.0~4.0 and the compressor stroke is within 10 mm~13 mm. At the piston stroke of 11 mm, the resonant frequencies are 38.3 Hz and 38 Hz and 37.8 Hz for pressure ratio of 4.0, 3.5 and 3.0.

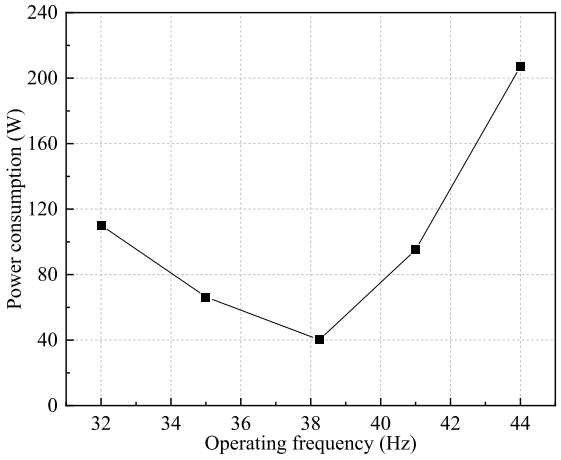

Fig. 14. Power consumption against operating frequency at condenser temperature of 50 °C, pressure ratio of 4.0 and input voltage of 50 V.

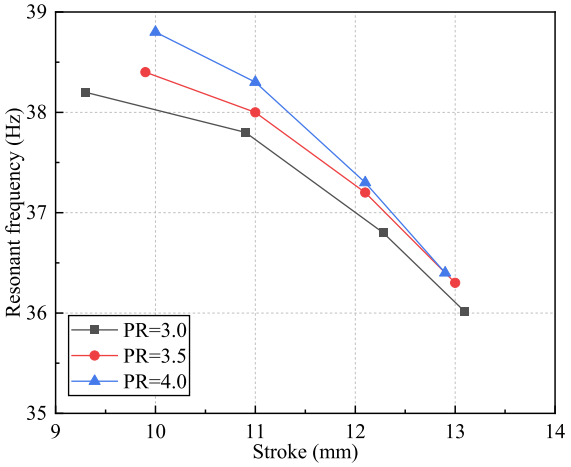

Fig. 15. Resonant frequency as a function of piston stroke.

Declaration of Competing Interest

The authors declare that they have no known competing financial interests or personal relationships that could have appeared to influence the work reported in this paper.

Data availability

Data will be made available on request.

References

[1] H. Jiang, K. Liang, Z. Li, Characteristics of a novel moving magnet linear motor for linear compressor, Mech. Syst. Sig. Process. 121 (2019) 828–840.
[2] K. Shao, J. Zheng, H. Wang, F. Xu, X. Wang, B. Liang, Recursive sliding mode control with adaptive disturbance observer for a linear motor positioner, Mech. Syst. Sig. Process. 146 (2021), 107014.
[3] Y. Zhao, J. Tan, B. Zhao, T. Zhang, H. Tan, R. Xue, S. Wu, Y. Zhai, H. Dang, Theoretical and experimental investigations on the piston offset characteristics in a four-stage DC linear compressor unit for a 1.8 K hybrid cryocooler, Int. J. Refrig 147 (2023) 153–162.
[4] W. Xu, X. Li, J. Zhu, Q. Wang, 3-d modeling and testing of a stator- magnet transverse-flux linear oscillatory machine for direct compressor drive, IEEE Trans. Ind. Electron. 68 (9) (2020) 8474–8486.
[5] Z. Lin, J. Wang, D. Howe, A learning feed-forward current controller for linear reciprocating vapor compressors, IEEE Trans. Ind. Electron. 58 (8) (2010) 3383–3390.
[6] Z. Zhu, K. Liang, Z. Li, H. Jiang, Z. Meng, Thermal-economic- environmental analysis on household refrigerator using a variable dis- placement compressor and low-gwp refrigerants, Int. J. Refrig 123 (2021) 189–197.
[7] X. Zhang, D. Ziviani, J.E. Braun, E.A. Groll, Theoretical analysis of dynamic characteristics in linear compressors, Int. J. Refrig 109 (2020) 114–127.

[8] J.K. Kim, C.G. Roh, H. Kim, J.H. Jeong, An experimental and numerical study on an inherent capacity modulated linear compressor for home refrigerators, Int. J. Refrig 34 (6) (2011) 1415–1423.
[9] X. You, L. Qiu, C. Duan, X. Jiang, C. Huang, X. Zhi, Study on the stroke amplitude of the linear compressor, Appl. Therm. Eng. 129 (2018) 1488–1495.
[10] Z. Shi, H. Xiao, Q. Zhu, Q. Wang, Resonant frequencies analysis and vibration control of fluid in three-dimensional (3D) moonpool: Analytical modeling and experimental study, Mech. Syst. Sig. Process. 144 (2020), 106882.
[11] M. Xia, X. Chen, Analysis of resonant frequency of moving magnet linear compressor of stirling cryocooler, Int. J. Refrig 33 (4) (2010) 739–744.
[12] H. Lee, S. S. Jeong, C. W. Lee, H. K. Lee, Linear compressor for air-conditioner, in: International Compressor Engineering Conference (2004) 1667.
[13] Z. Lin, J. Wang, D. Howe, A resonant frequency tracking technique for linear vapor compressors, IEEE International Electric Machines & Drives Conference 1 (2007) (2007) 370–375.
[14] C.R. Bradshaw, A miniature-scale linear compressor for electronics cooling, Purdue University, 2012. Ph.D. thesis.
[15] K. Liang, A review of linear compressors for refrigeration, Int. J. Refrig 84 (2017) 253–273.
[16] M.H. Yu, Y.Q. Zhang, Y.Y. Ye, Z.Y. Yao, Q.F. Lu, Research on resonant frequency tracking strategy for linear oscillatory motor, in: In: Proceedings of the 29th Chinese Control Conference, 2010, pp. 3348–3352.
[17] W. Xu, Q. Wang, X. Li, Y. Liu, J. Zhu, A novel resonant frequency tracking control for linear compressor based on mras method, CES Transactions on Electrical Machines and Systems 4 (3) (2020) 227–236.
[18] T. Suzuki, M. Koyama, S. Nagata, W. Hatsuse, M. Takemoto, S. Ogasawara, Resonant frequency tracking control for a linear compressor with assist springs, in: In: 2020 IEEE Energy Conversion Congress and Exposition (ECCE), 2020, pp. 3016–3021.
[19] T. W. Chun, J. R. Ann, J. Y. Yoo, C. W. Lee, Analysis and control for linear compressor system driven by pwm inverter, in: 30th Annual Conference of IEEE Industrial Electronics Society, IECON 1 (2004) 263–267.
[20] T. Zhang, H. Yu, A novel strategy of resonant frequency tracking control for linear compressor, in: In: 2017 20th International Conference on Electrical Machines and Systems (ICEMS), 2017, pp. 1–6.
[21] T.W. Chun, J.R. Ahn, H.H. Lee, H.G. Kim, E.C. Nho, A novel strategy of efficiency control for a linear compressor system driven by a pwm inverter, IEEE Trans. Ind. Electron. 55 (1) (2008) 296–301.
[22] J. Latham, M.L. McIntyre, M. Mohebbi, Parameter estimation and a series of nonlinear observers for the system dynamics of a linear vapor compressor, IEEE Trans. Ind. Electron. 63 (11) (2016) 6736–6744.
[23] J. Latham, M.L. McIntyre, M. Mohebbi, Sensorless resonance tracking and stroke control of a linear vapor compressor via nonlinear observers, IEEE Trans. Ind. Electron. 65 (5) (2017) 3720–3729.
[24] W. Xu, Q. Wang, Y. Liu, X. Li, K. Liao, Adaptive full-order displacement observer for sensorless resonant frequency tracking control of linear oscillatory machines, IEEE Trans. Ind. Electron. 69 (2) (2021) 1310–1321.
[25] N. REFRPOP, Reference fluid thermodynamic and transport properties database, Software Package, Ver 9 (2023).
[26] K. Liang, A novel linear electromagnetic-drive oil-free refrigeration com- pressor, University of Oxford, 2014. Ph.D. thesis.
[27] N. Wang, S.F. Su, Finite-Time Unknown Observer-Based Interactive Trajectory Tracking Control of Asymmetric Underactuated Surface Vehicles, IEEE Trans. Control Syst. Technol. 29 (2) (2021) 794–803.
[28] N. Wang, C. Qian, J.C. Sun, Y.C. Liu, Adaptive Robust Finite-Time Trajectory Tracking Control of Fully Actuated Marine Surface Vehicles, IEEE Trans. Control Syst. Technol. 24 (4) (2016) 1454–1462.
[29] Z. Li, Measurements and modelling of a novel oil-free refrigeration system, University of Sussex, 2020. Ph.D. thesis.
[30] Z. Zhu, K. Liang, Z. Li, H. Jiang, Z. Meng, A numerical model of a linear compressor for household refrigerator, Appl. Therm. Eng. 198 (2021), 117467.